

# Learning Driver Braking Behavior using Smartphones, Neural Networks and the Sliding Correlation Coefficient: Road Anomaly Case Study

Christopoulos, S, Kanarachos, S & Chroneos, A

Author post-print (accepted) deposited by Coventry University's Repository

**Original citation & hyperlink:**

Christopoulos, S, Kanarachos, S & Chroneos, A 2018, 'Learning Driver Braking Behavior using Smartphones, Neural Networks and the Sliding Correlation Coefficient: Road Anomaly Case Study' *IEEE Transactions on Intelligent Transportation Systems*, vol (in press), pp. (in press)

<https://dx.doi.org/10.1109/TITS.2018.2797943>

DOI [10.1109/TITS.2018.2797943](https://dx.doi.org/10.1109/TITS.2018.2797943)

Print ISSN: 1524-9050

Electronic ISSN: 1558-0016

Publisher: IEEE

**© 2018 IEEE. Personal use of this material is permitted. Permission from IEEE must be obtained for all other uses, in any current or future media, including reprinting/republishing this material for advertising or promotional purposes, creating new collective works, for resale or redistribution to servers or lists, or reuse of any copyrighted component of this work in other works.**

Copyright © and Moral Rights are retained by the author(s) and/ or other copyright owners. A copy can be downloaded for personal non-commercial research or study, without prior permission or charge. This item cannot be reproduced or quoted extensively from without first obtaining permission in writing from the copyright holder(s). The content must not be changed in any way or sold commercially in any format or medium without the formal permission of the copyright holders.

This document is the author's post-print version, incorporating any revisions agreed during the peer-review process. Some differences between the published version and this version may remain and you are advised to consult the published version if you wish to cite from it.

# Learning Driver Braking Behavior using Smartphones, Neural Networks and the Sliding Correlation Coefficient: Road Anomaly Case Study

Stavros-Richard G. Christopoulos, Stratis Kanarachos, and Alexander Chroneos

**Abstract**—The present study focuses on the automated learning of driver braking “signature” in the presence of road anomalies, using smartphones. Our motivation is to improve driver experience using preview information from navigation maps. Smartphones facilitate, due to their unprecedented market penetration, the large-scale deployment of Advanced Driver Assistance Systems (ADAS). On the other hand, it is challenging to exploit smartphone sensor data because of the fewer and lower quality signals, compared to the ones on board. Methods for detecting braking behavior using smartphones exist, however, most of them focus only on harsh events. Additionally, only a few studies correlate longitudinal driving behavior with the road condition. In this paper, a new method, based on deep neural networks and the sliding correlation coefficient, is proposed for the spatio-temporal correlation of road anomalies and driver behavior. A unique Deep Neural Network structure, that requires minimum tuning, is proposed. Extensive field trials were conducted and vehicle motion was recorded using smartphones and a data acquisition system, comprising an IMU and differential GPS. The proposed method was validated using the probabilistic Receiver Operating Characteristics method. The method proves to be a robust and flexible tool for self-learning driver behavior.

**Index Terms**—Advanced Driver Assistance Systems, Braking behavior, Neural Networks, Smartphones, Road condition.

## I. INTRODUCTION

Over the last decade, mobile phones, transformed from simple cell devices for making calls, to powerful sensing, communication and computing devices [1]. First, smartphones have numerous sensors embedded, for example, GPS, accelerometers, gyroscope and magnetometer [2]. Second, the upcoming 5th generation of wireless systems (5G) will provide high quality and uninterrupted mobile services [3]. Third, it is

estimated that by 2020, 70% of earth's population will be a smartphone user [4]. In this context, smartphones can facilitate the rapid and large-scale deployment of Intelligent Transportation Applications (ITS) [5].

Smartphones are increasingly exploited for monitoring driver behavior [6]. Some recent examples include Singht *et al.* who detected sudden braking and lateral maneuvers by analyzing vehicle motion using Dynamic Time Warping [7]. Predic and Stojanovic [8] classified driver behavior by correlating driving data to pre-recorded samples. Castignani *et al.* [9] assigned driving scores using smartphone data and fuzzy logic. Saiprasert *et al.* monitored over-speeding as a means to classify risky driving [10]. Insurance industry is responding to this trend by gradually introducing smartphone-based Pay-as-You-Drive schemes [11].

Although the usage of smartphones for ITS is desirable, there are standard challenges that need to be overcome. These are the free position of a smartphone in the vehicle, the low accuracy of GPS position/speed signals in urban areas and the high noise to signal ratio in the accelerometer/gyroscope signals. Regarding the first, some applications require mounting the smartphone at a fixed position or dynamically reorienting its axes by real-time computing the Euler angles. The Euler angles are computed using the magnetometer readings and the direction of gravity or by using the longitudinal, lateral and vertical acceleration along the smartphone's axes [12]-[13]. Smartphone GPS signal accuracy was studied in [14]. In general, smartphone GPS measurements were consistent. However, in obscured environments the deviation from ground truth deteriorated by a factor of two. Crowdsensing and 5G technology will considerably improve positioning accuracy in urban areas [15]. With respect to the noisy accelerometer and gyroscope signals, these can heavily affect driving analytics. To this end, many methods depending on the end application have been proposed [16].

The present study focuses on driver comfort and particularly on modeling the driver braking behavior in the presence of

This work was supported by Intelligent Variable Message Systems (iVMS), funded by the Government's Local Growth Fund through Coventry and Warwickshire Local Enterprise Partnership

S.-R. G. Christopoulos is with Faculty of Engineering, Environment and Computing, Coventry University, Priory Street, Coventry CV1 5FB, United Kingdom. He is also with Solid Earth Physics Institute, Faculty of Physics, National and Kapodistrian University of Athens, Panepistimiopolis, Zografos 157 84, Athens, Greece (e-mail: [ac0966@coventry.ac.uk](mailto:ac0966@coventry.ac.uk)).

S. Kanarachos is with Faculty of Engineering, Environment and Computing, Coventry University, Priory Street, Coventry CV1 5FB, United Kingdom (e-mail: [ab8522@coventry.ac.uk](mailto:ab8522@coventry.ac.uk)).

A. Chroneos is with Faculty of Engineering, Environment and Computing, Coventry University, Priory Street, Coventry CV1 5FB, United Kingdom (e-mail: [ab8104@coventry.ac.uk](mailto:ab8104@coventry.ac.uk)).

discrete road anomalies. Most of the studies, found in the literature, focus either on braking for safety or on road anomalies detection without considering the human element. We extend the usual scope of analysis by correlating driver behavior and road condition. The aim is to learn driver preferences so that an intelligent ADAS adapt and maximize driver comfort, when preview map information is used [17].

To this end, a flexible method is required that can adapt to human subject response and vehicle characteristics. We propose a data-based method using a unique Deep Neural Network structure, suitable for the analysis of multivariate time series [18], [19]. Extensive field trials, using different vehicles and drivers, demonstrated that the method performs robustly and requires minimum tuning. Furthermore, it is the first time that a new visualization scheme can reveal in one figure a driver's braking preferences for different types of road anomalies and speeds. This method can be extended to other scenarios like braking before turning.

The rest of the paper is structured as follows: in section 2 studies on smartphone-based road condition monitoring are reviewed. Section 3 describes the experimental part. Section 4 describes the Anomaly Detection Filter (ADF), while in section 5 the sliding correlation coefficient is applied and numerical results are discussed. Finally, in section 6, we set out the conclusions obtained and discuss future steps.

## II. RELATED WORK: ROAD CONDITION MONITORING

One of the first contributions in the field of smartphone-based road condition monitoring was Nericell [20]. Nericell utilized a GPS receiver, GSM for cellular localization and a 3-axis accelerometer sensor. The acceleration signal was sampled at 310 Hz, a rate which is high even with today's standards. To detect braking incidences, the mean of longitudinal acceleration  $a_x$  was calculated over a sliding window. When the mean value exceeded a predefined threshold, a braking event was declared. The ground truth was established using the GPS signal, despite that GPS signal is not always accurate. For bump detection, two different criteria were employed, depending on the speed of the vehicle. At speeds, greater than 7 m/s the surge in vertical acceleration  $a_z$  was used. When the spike along the vertical acceleration signal  $a_z$  was greater than a predefined threshold  $T_2$ , a bump was declared. At speeds, lower than 7 m/s the algorithm searched for a sustained dip in  $a_z$ , reaching below a threshold  $T_3$  and lasting at least 20 ms. The detection of road anomalies at low speeds was less successful, as stated in [12].

Perttunen *et al.* detected road anomalies by recording the acceleration signal at 38Hz and GPS position at 1 Hz [21]. The raw signals were filtered by applying a Kalman filter. Subsequently, features were extracted using sliding windows. The standard deviation, mean value, variance, peak-to-peak value, signal magnitude area, 3<sup>rd</sup> order autoregressive coefficients, tilt angles and root mean square for each dimension of the acceleration signal and the correlation between the signals in all dimensions were calculated. Additional features were used by extracting the Fast Fourier Transformation energy from 17 frequency bands in each

acceleration direction. A linear transformation was applied to make the features speed independent. Support Vector Machines (SVMs) were applied to perform the classification. Support Vector Machines is a supervised machine learning method, requiring labeling of all road anomalies. Ground truth was produced using two independent labelers. The best performance achieved 82% sensitivity and 18% false negatives rate.

Douangphachanh and Oneyama presented a method for estimating the International Roughness Index (IRI) of road segments using smartphones [22]. Four different cars were used in the experiments and two smartphones at different positions in the vehicle. The sampling rate was 100 Hz. At this rate, the smartphone's processing power is almost exclusively used for the measurement purpose. The raw data were pre-processed using a high pass filter. It was assumed that road anomalies cause only high frequency accelerations. A linear relationship between IRI and the magnitude of acceleration signal at specific frequency bands was derived. Correlation ranged between 0.6 and 0.78. A road survey vehicle was used to generate the ground truth. IRI was estimated for 100 m long road sections, which is rather too long for discovering discrete road anomalies.

Vittorio *et al.* proposed a threshold-based method [12]. The accelerometer and GPS data were transferred at 1 Hz frequency to a central server. First, the data were filtered to remove the low frequency components. Then the minimum, average and maximum acceleration values of every batch of measurements was calculated. The high-energy events were identified by observing the vertical acceleration impulse and comparing it to, heuristically derived, thresholds. The algorithm's best performance achieved more than 80% correct positive road anomalies classifications and 20% percentage of false positives.

MAARGHA, developed by Rajamohan *et al.*, is different to the aforementioned approaches because it employed image processing [23]. Images using the smartphone camera were captured at a frequency 0.5 Hz. The focus was 1 – 2 m ahead of the vehicle. The GPS location and speed were sampled at 1 Hz. The accelerometer was sampled at 15 Hz. Features were extracted in sliding windows, 2s long. A high pass filter was employed to the raw signal. Classification was performed using the *K*-Nearest Neighbor (*K*-NN) algorithm. Under clear sky the classification was 100% accurate, while in segments where the road was laden with shadows of buildings the accuracy degraded to roughly 50%.

In conclusion, none of the above studies attempted to correlate longitudinal driving behavior and the road condition. However, drivers have different responses depending on the road anomalies, driving style and vehicle. This study, attempts to fill this gap, using a flexible method based on a widely available tool, the smartphone.

## III. EXPERIMENTAL PART

### A. Smartphone-based data acquisition

Three different smartphones were used in the field trials. All smartphones were equipped with GPS receivers. They also comprised a tri-axial accelerometer and tri-axial electronic compass. The smartphone was positioned on the box behind the

gearbox handle, see Fig. 1. A Gecko pad was used to minimize any relative movement between the smartphone and the vehicle. The sampling rate for the accelerometer, gyro and compass sensors was 10 Hz. The sampling frequency of GPS position and velocity was 1 Hz. The vehicle speed in urban areas ranged between 2.7-11.1 m/s. The maximum vehicle speed was 16.6 m/s. At higher speeds anomaly detection becomes rather straightforward due to the intensity of the event.



Fig. 1: Smartphone position during the field trials

### B. Instrumented vehicle data acquisition system

The test vehicle is a Ford Fiesta equipped with a motion data acquisition system, VBOX 3i data logger with dual antenna. The data logger uses a GPS/GLONASS receiver, logging data 100 times a second. An inertial measurement unit (IMU) is integrated into VBOX and a Kalman Filter is implemented to improve all parameters measured in real-time. Velocity and heading data were calculated from the Doppler Shift effect in the GPS carrier signal. The following CAN-bus signals were also logged: engine speed, steering angle, gear position, throttle pedal position, brake pedal position, brake pedal (on/off), clutch pedal, handbrake, wheel speeds, vehicle longitudinal acceleration and vehicle lateral acceleration. Video recording took place during the field trials. The signals obtained from VBOX in combination with the video footages were used to generate the ground truth.

### C. Test Routes

Three experiments were conducted. The first experiment was carried out on a route at the center of Coventry City (Fig. 2). The driver drove the same route from point A to point B five times, following five different braking behaviors (a) no braking, (b) braking over and just after, (c) just before, (d) “normally before” and, (e) “quite before” the road “anomalies”. The second experiment was carried out with additional drivers at a different location, the campus of the National and Technical University of Athens, Greece. The campus contains several speed bumps, at known positions. The location was chosen because it was easier for the driver to follow different average speeds and the route also has significant road slope that may potentially mislead the classifier. The third experiment was conducted to monitor the naturalistic behavior of drivers. It was held at various locations including Coventry City entry routes, U.K. and Zografou-Iliissia, Greece.

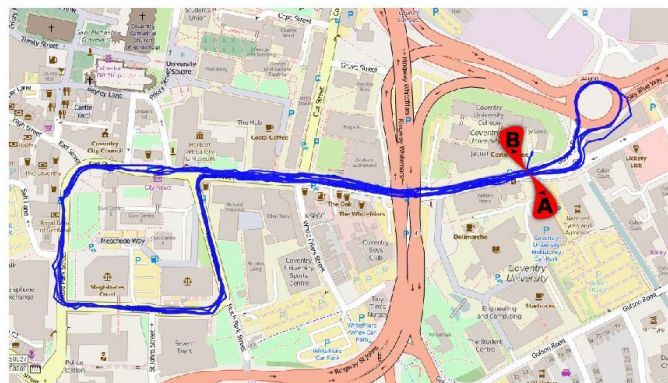


Fig. 2. (color online) Vehicle route (blue line) in Experiment I. Field trials were conducted in Coventry.

### D. Data collection - Ground truth

During the experiments, the X and Z-axis acceleration from VBOX and the position of the pedal brake from the OBDII port were extracted. Simultaneously, we recorded the X and Z-axis acceleration data using the smartphone sensors. Thus, for each route, we constructed files with the following columns: Time, X-axis acceleration that extracted from VBOX, Z-axis acceleration that extracted from VBOX, braking pedal position that extracted from VBOX, X-axis acceleration that extracted from smartphone sensor and Z-axis acceleration that extracted from smartphone sensor. As ground truth, we used the data extracted from VBOX and OBDII port. Additionally, video recordings of the road segment ahead of the vehicle supplemented with audio comments were collected.

## IV. ANOMALY DETECTION FILTER

The Anomaly Detection Filter (ADF) is based on the Deep Neural Networks (DNNs) paradigm. DNNs have not been extensively applied in time series modeling, but recent applications in other areas demonstrated their potential [24]. In [19] DNNs were applied for the first time in the detection of road anomalies. The architecture of the DNN is presented in Fig. 3. The ADF comprises 5 steps. In the first step the signal is de-noised. In the second step, a subset of the time series is used to train the DNN. The subset corresponds to data generated in a smooth ride. In the third step, the error between the de-noised time series and the one generated by DNNs is calculated. In the fourth step the Hilbert transform of the error signal is computed. In the fifth step the ADF outcome is derived.

This study further develops [19] by detecting also braking events and correlating them to the vertical vehicle response.

### A. Signal decomposition

The first step in the proposed method is the decomposition of a time series  $x(t)$  using wavelets. Wavelets can detect anomalies of short duration better than the Fourier transform [25]. Furthermore, they analyze a signal in multiple scales, a very useful property for distinguishing nonlinear signals. For example, Fig. 4 presents the spread of Holder exponents obtained when analyzing the acceleration signal for a smooth (red color) and an anomalous road segment (blue color). A

signal  $x(t)$  is decomposed into different levels of detail, by convolving wavelet  $\psi_{m,n}$  and signal  $x(t)$ :

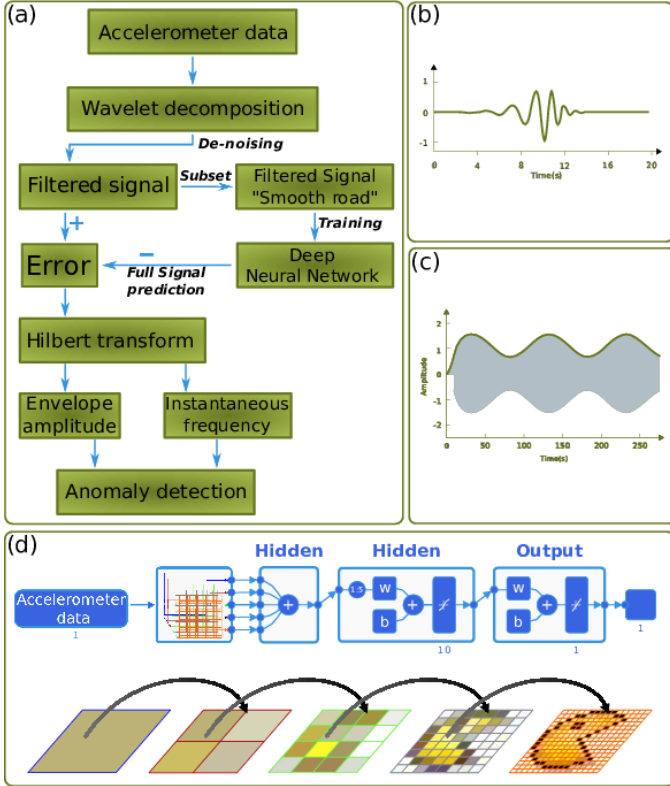


Fig. 3. (color online) Anomaly Detection Filter algorithm: a) Flow chart b) Daubechies 9 wavelet basis for de-noising the raw signal c) Energy temporal evolution d) Deep neural network architecture for learning the patterns in and between different time scales.

$$\psi_{m,n}(t) = 2^{-m/2} \cdot \psi \cdot (2^{-m} \cdot t - n) \quad (1)$$

$$T_{m,n} = \int_{-\infty}^{\infty} x(t) \cdot \psi_{m,n}(t) \cdot dt \quad (2)$$

where  $T_{m,n}$  are the discrete wavelet transform values given on a scale-location grid of index  $m,n$ . The integers  $m,n$  control the wavelet dilation and translation respectively. The inverse discrete wavelet transform reconstructs signal  $x(t)$  using coefficients  $T_{m,n}$  and the wavelet basis  $\psi_{m,n}$ :

$$x(t) = \sum_{m=-\infty}^{\infty} \sum_{n=-\infty}^{\infty} T_{m,n} \cdot \psi_{m,n}(t) \quad (4)$$

To obtain a multi-resolution of signal  $x(t)$ , the use of a scaling function  $\varphi(t)$  is necessary:

$$\varphi_{m,n}(t) = 2^{-m/2} \cdot \varphi \cdot (2^{-m} \cdot t - n) \quad (5)$$

$$\int_{-\infty}^{\infty} \varphi_{0,0}(t) \cdot dt = 1 \quad (6)$$

The scaling function is convolved with signal  $x(t)$  to produce the approximation coefficients  $S_{m,n}$ :

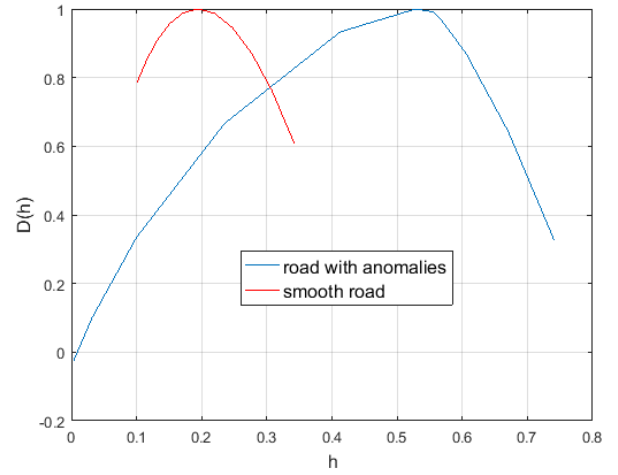


Fig. 4: (color online) Multifractal analysis: Spread of the Holder exponent values for a road segment with (blue) and without anomalies (red).

$$S_{m,n} = \int_{-\infty}^{\infty} x(t) \cdot \varphi_{m,n}(t) \cdot dt \quad (7)$$

and obtain a continuous approximation of signal  $x_m(t)$ , at scale  $m$ :

$$x_m(t) = \sum_{-\infty}^{\infty} S_{m,n} \cdot \varphi_{m,n}(t) \quad (8)$$

where  $x_m(t)$  is the approximation of signal  $x(t)$ , at scale  $m$ . Combining Equations (4) & (8), signal  $x(t)$  becomes:

$$x(t) = \sum_{n=-\infty}^{n=\infty} S_{m_0,n} \cdot \varphi_{m_0,n}(t) + \sum_{m=-\infty}^{m_0} \sum_{n=-\infty}^{\infty} T_{m,n} \cdot \psi_{m,n}(t) \quad (9)$$

If  $d_m(t)$  is the signal detail, at scale  $m$ :

$$d_m(t) = \sum_{n=-\infty}^{\infty} T_{m,n} \cdot \psi_{m,n}(t) \quad (10)$$

then (9) is rewritten as:

$$x(t) = x_{m_0}(t) + \sum_{m=-\infty}^{m_0} d_m(t) \quad (11)$$

$$x_{m-1}(t) = x_m(t) + d_m(t) \quad (12)$$

Equation (12) describes how to obtain the multiresolution analysis of the signal. The signal approximation  $x_{m-1}(t)$  is obtained if the signal detail  $d_m(t)$ , at an arbitrary scale  $m$ , is added to the approximation  $x_m(t)$  at that scale.

To remove noise from signal  $x(t)$ , a threshold  $\lambda$  is defined and the detail coefficients  $T_{m,n}$  are adjusted according to:

$$T_{m,n} = \begin{cases} 0, & \text{if } |T_{m,n}| < \lambda \\ T_{m,n}, & \text{if } |T_{m,n}| \geq \lambda \end{cases} \quad (13)$$

$$x_d(t) = x_{m0}(t) + \sum_{m=-\infty}^{m0} d_{dm}(t) \quad (14)$$

where  $d_{dm}(t)$  is the filtered signal detail, at scale  $m$ .

Different wavelet bases were investigated and among  $db2$ ,  $db3$ ,  $db4$ ,  $db5$ ,  $db6$ ,  $db7$ ,  $db8$ ,  $db9$ , and  $db10$ ,  $db9$  achieved the best performance. Fig. 5 shows the distance, obtained using Dynamic Time Warping, between the different wavelet bases and the sample signal utilized for training the DNN.

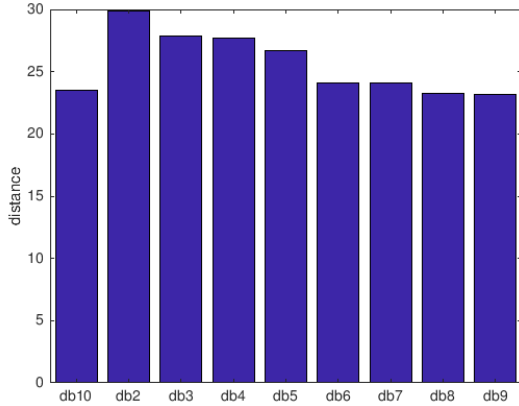


Fig. 5: a) Distance, using dynamic time warping, between wavelet bases  $db2$ ,  $db3$ ,  $db4$ ,  $db5$ ,  $db6$ ,  $db7$ ,  $db8$ ,  $db9$ , and  $db10$  and the training signal.

### B. Deep Neural Network structure

The signals extracted using the wavelet analysis feed a DNN, that is trained to predict  $x_d$ . The training data for the DNN are obtained while driving on smooth and slightly rough road segments. No intense braking events are included in the training data. Eventually, semi-supervised learning is employed; only training data relevant to smooth and slightly rough road conditions are included. Thus, it is not required to collect and record road anomalies for training the DNN, as is required in other methods e.g. SVMs. For the application deployment, a calibration phase is required during which the driver classifies the road condition or driving behavior as normal. In the calibration phase, the weighted acceleration according to ISO 2631-1:1997 is also calculated with the purpose to normalize driver's subjective input.

DNN's architecture is shown in Fig. 3(d). The first part is a set of stacked NNs that models the filtered time series  $x_d$  at different time scales. The second part is an autoregressive NN consisting of 10 hidden layers with nonlinear (log-sigmoid) activation functions and a three-layer buffer. Although the exact number of hidden layers and buffer size are problem-dependent it was found that relatively simple NNs (number of hidden layers less than five) cannot represent the temporal dynamics sufficiently. Numerical trials using buffers of different sizes have shown that a large buffer size decreases the detector's performance. A buffer of size three achieved the best performance.

Among the different training algorithms examined – including the 1) Broyden–Fletcher–Goldfarb–Shanno (BFGS) Quasi-Newton algorithm, 2) Bayesian Regularization (BR), 3) Gradient descent with adaptive learning rate backpropagation (GDA), 4) Gradient descent with momentum backpropagation (GDM) and 5) Levenberg-Marquardt backpropagation (LM) - LM achieved the best performance. All training algorithms were repetitively applied (30 iterations). Fig. 6 shows the results of the Kruskal-Wallis test.

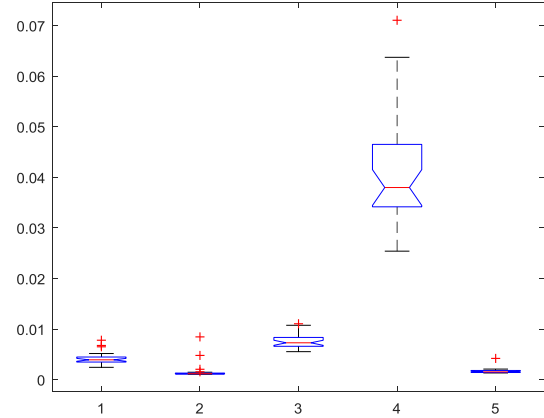


Fig. 6: Results of Kruskal –Wallis test for different NN training algorithms: Bayesian Regularization (2) and Levenberg-Marquardt (5) achieve the best performance

### C. Anomaly detection using Hilbert transform

The error signal  $e$  is defined as the difference of the filtered signal  $x_d(t)$  from DNN's output  $y(t)$ :

$$e = x_d - y \quad (19)$$

The features utilized for detecting the road anomaly and braking events are the envelope  $A$  and instantaneous frequency  $\hat{\theta}(t)$  of the error signal  $e(t)$ . For this the Hilbert transform is utilized:

$$e_H(t) = \lim_{\epsilon \rightarrow 0} \left[ \frac{1}{\pi} \cdot \int_{-\infty}^{t-\epsilon} \frac{e(t)}{x-t} \cdot dt + \frac{1}{\pi} \cdot \int_{t+\epsilon}^{+\infty} \frac{e(t)}{x-t} \cdot dt \right] \quad (20)$$

where  $e_H(t)$  is the Hilbert transform. Hilbert transform is the convolution of  $e(t)$  with a reciprocal function  $1/x - t$ , thus Hilbert transform emphasizes the local properties of  $e(t)$ . If  $\hat{e}(\omega)$  represents the Fourier transform of  $e(t)$ , then the Hilbert transform is:

$$e_H(t) = \mathcal{F}^{-1}\{-j \cdot \text{sgn}(\omega) \cdot \hat{e}(\omega)\} \quad (21)$$

where  $\mathcal{F}^{-1}$  represents the inverse Fourier transform [26]. The instantaneous phase  $\theta(t)$ , frequency  $\hat{\theta}(t)$ , and amplitude  $A(t)$  of  $e(t)$  are defined:

$$\theta(t) = \arctan \left\{ \frac{e_H(t)}{e(t)} \right\} \quad (22)$$

$$\dot{\theta}(t) = \frac{d\theta}{dt}$$

$$A(t) = \sqrt{e(t)^2 + e_H(t)^2} \quad (23)$$

Hilbert transform is useful for identifying instantaneous frequency changes in the higher frequency spectrum, in which wavelet transform is not performing well. When the instantaneous frequency is not informative the signal's envelope is exploited instead.

## V. DISCOVERING DRIVER BRAKING BEHAVIOR

Three different experiments were carried out for identifying and correlating the driver braking behavior to the road condition. The first experiment aims to verify five driver braking behaviors. The second experiment aims to identify the braking behavior for different drivers and driving styles (passive-normal-aggressive). The third experiment aims to identify the braking behavior when driving naturally.

In all cases, using the ADF, we try to identify marked changes to the  $X$  and  $Z$ -axis acceleration.

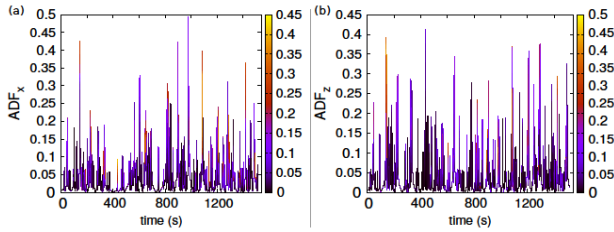


Fig. 7. (color online) Combination of the results of the Anomaly Detection Filter (ADF) after the analysis of the entire time series of the accelerometer of the smartphone for two different perspectives: (a) The ADF value of  $X$ -axis ( $ADF_x$ ) versus time whereas the color represents the ADF value of  $Z$ -axis ( $ADF_z$ ) and (b)  $ADF_z$  versus time whereas the color represents the  $ADF_x$ .

In Figs 7 (a) and (b) the results of the ADF – for the first experiment – after the analysis of the smartphone acceleration data in the longitudinal  $x$  and vertical direction  $z$  are presented.

### A. Evaluation of ADF filter

As a first step, we estimated the efficiency of the ADF. We employed, for this reason, the ROC diagram [27]. The value  $e$  of ADF can be used here as an estimator [28] and the  $M$  as an index which value is equal to one ( $M = 1$ ) when there is an “anomaly” and zero ( $M = 0$ ) when there is not. Thus, we examine if the value  $e$  of ADF lies over different values of threshold  $e_i$ . The ROC graph depicts the True Positive rate ( $TPr$ ) on  $Z$ -axis and the False Positive rate ( $FPr$ ) on the  $X$ -axis. Therefore, there are four classifications (a)  $TP$  (True Positive) when  $e \geq e_i$  and  $M = 1$ , (b)  $FP$  (False Positive) when  $e \geq e_i$  and  $M = 0$ , (c)  $FN$  (False Negative) when  $e < e_i$  and  $M = 1$  and, (d)  $TN$  (True Negative) when  $e < e_i$  and  $M = 0$ . Thus, the  $TPr$  represents the ratio  $TP/(TP+FN)$ , and the  $FPr$  the ratio  $FP/(FP+TN)$ . A schematic representation of ROC analysis is shown in Fig. 8. For a random estimator the curve is located close to the diagonal, where  $TPr$  and  $FPr$  are roughly equal. A popular measure is the area under the ROC curve (AUC)[39]. Additionally, we can use the recently proposed visualization scheme based on  $k$ -ellipses, for the examination of the statistical

significance of the results [29]. With this technique, using the AUC of  $k$ -ellipses we can measure the  $p$ -value of the probability to obtain a ROC curve by chance for given values of the total of positives  $P=TP+FN$  and the total of negatives  $Q=FP+TN$ , when ascribing  $e \geq e_i$  or  $e < e_i$  are random.

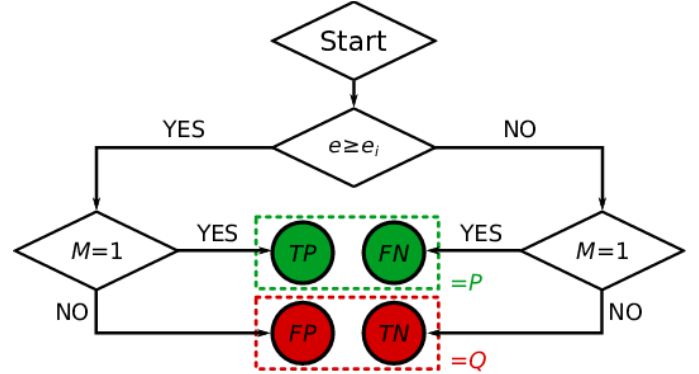


Fig. 8: Schematic representation of ROC analysis

In Fig. 9 the very good efficiency of the “braking” detection using the above method is illustrated. The present ROC analysis was held taking as the threshold a value of the braking pedal position obtained from OBDII. The range of position values obtained was 0 to 60, thus the thresholds  $B_i$  that we chose for the evaluation were equal to 20 and 30. Thus, when the value is greater or equal to the threshold then  $M = 1$ , otherwise  $M = 0$ . When  $B_i$  is equal to 20 the value of AUC is 0.87 and when  $B_i$  is equal to 30 the value of AUC is 0.97; the  $p$ -values of the corresponding  $k$ -ellipses in both cases are much smaller than  $10^{-8}$ . The fact that we obtain (Fig. 9)  $TPr \approx 75\%$  with  $FPr \approx 16.3\%$  when  $B_i = 20$  and  $TPr \approx 91.5\%$  with  $FPr \approx 3.0\%$  when  $B_i = 30$ , allowed us to employ the ADF for detecting braking events.

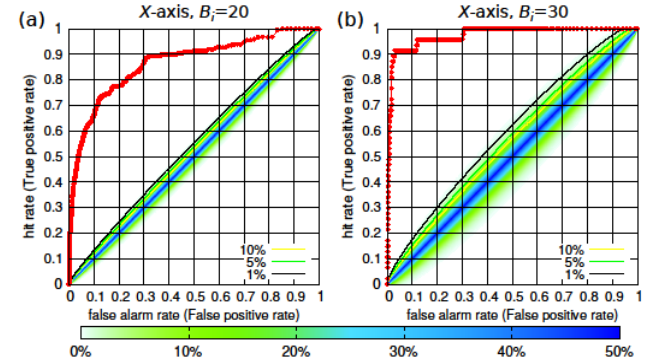


Fig. 9. (color online) ROC (red circles) of  $ADF_x$  when using the threshold (a)  $B_i = 20$  and (b)  $B_i = 30$ , that corresponds to the braking pedal position, as an estimator for the detection of marked changes in driver speed. The  $k$ -ellipses with  $p$ -value equal to 1%, 5% and 10% are drawn with black, green and yellow solid lines respectively.

Recently, the application of the ADF filter in the detection of road “anomalies” showed similar performance [19]. The  $p$ -values of the corresponding  $k$ -ellipse was much smaller than  $10^{-8}$  and for  $TPr$  around 80.6% the  $FPr$  was 11.7%. Hence, these outcomes allowed us to use the ADF for detecting road anomalies.

### B. Methodology

To discover the dependence of driving behavior on road

anomalies, we examined the correlation between the “anomalies” of ADF output on  $X$  and  $Z$  axes. Given the fact that the data is not Gaussian, we used the Spearman correlation coefficient  $r_s$ , which is a nonlinear statistical measure [30]:

$$r_s = \frac{\sum_i (x_i - \bar{x})(z_i - \bar{z})}{\sqrt{\sum_i (x_i - \bar{x})^2 \sum_i (z_i - \bar{z})^2}} \quad (21)$$

$r_s$  ranges  $r_s \in [-1,1]$ . When  $r_s$  is close to 1 the correlation is “strong”, while for positive values close to 0 it is “weak”.  $r_s$  close to  $-1$  indicates “strong” anti-correlation.

The method is described as follows. First, we calculate the Spearman’s correlation coefficient between the segment of the time series of ADF on  $Z$ -axis and the corresponding  $X$ -axis segment slid backwards by  $n$  positions (i.e.  $\Delta t = n/10$  s). Subsequently, we slide forward this segment of  $X$ -axis by one, two, ...,  $2n - 1$  (in the following experiments  $n = 50$ ) positions and calculate the correlation for each position. Finally, we repeat the same procedure for a range of thresholds  $T_z$  of the ADF output on  $Z$ -axis corresponding to the different sizes of the road “anomalies”. The range of thresholds is from 0 to the maximum value of the outcome of ADF output on  $Z$ -axis, equally divided by 100. In more detail, for a given threshold  $T_z$  we are taking the time series of the ADF output on  $Z$ -axis, which are greater than  $T_z$  together with the corresponding time series on  $X$ -axis, see Fig. 10.

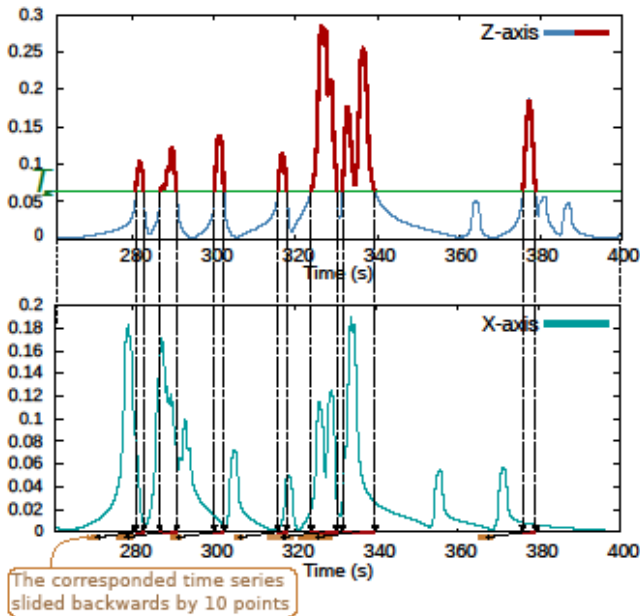


Fig. 10: (color online) Schematic representation of the correlation coefficient calculation for a given threshold  $T_z$ . The red line denotes the segments of the initial  $Z$ -axis time series that exceed the threshold  $T_z$  and the corresponding time series on the  $X$ -axis slid by 10 points (brown color).

### C. Experimental process

#### Experiment 1:

The aim of the first experiment is to examine if the proposed method can discover distinct driving patterns. In this experiment, the car followed the route indicated in Fig. 2. We

performed the same route from point A to point B five times, following five distinct driving patterns (a) no braking, (b) braking over and just after, (c) just before, (d) “normally before” and, (e) “quite before” the road “anomalies”.

The application of the methodology, described in the previous section, led to a successful discovery of the distinct driving patterns. The results are shown in Figs 11 (a), (b), (c), (d) and (e), where yellow indicates the “strong” correlation coefficient and the black-purple, the “strong” anti-correlation coefficient, while, with red indicated the “weak” correlation and anti-correlation coefficient. At this point, it is appropriate to describe each route separately.

In the first route (A1), the driver (Driver A) applied the brakes immediately after passing the road “anomalies”. We observe in Fig. 11(a) that there is “strong” anti-correlation coefficient before and over the road “anomalies”, while, there is “strong” correlation coefficient after. Interestingly, we observe that for the small obstacles or potholes ( $T_z \leq 0.2$  m/s<sup>2</sup>), the driver kept on driving without braking.

In the second route (A2), the driver attempted to brake while passing the road anomaly, but the human response time resulted in braking immediately after. As in the first route, the results in Fig. 11(b) are consistent with the reality. The driver was removing the foot from the accelerator pedal approximately, 1.1s before the obstacle or the pothole.

In the third route (A3), the driver was braking just before the “anomalies”. This behavior is clearly depicted in Fig. 11(c). Additionally, the results indicate that the driver was not braking for small “anomalies” and that the foot was removed from the acceleration pedal about 1.1 sec before the application of brakes.

Finally, in the fourth (A4) and fifth (A5) routes, the driver was braking “normally before” and “quite before” the road “anomalies”. The diagrams in Figs 11(d) and (e) confirm these patterns.

#### Experiment 2:

In the second experiment additional drivers were used and a wider range of average speeds was achieved. Two additional drivers, Driver B and Driver C, were asked to drive a route in Politechniopolis campus, Zografos, Greece. The campus features road bumps at known locations. Road slope within the campus varies significantly. Both drivers performed three trials (Driver B: routes B1, B2, B3 and Driver C: C1, C2, C3), each with a different driving style and average speed (i.e. low, medium and high).

At low and medium speeds, Driver B was usually braking at approximately 0.7s before the road “anomaly” and “just before” the obstacle (Figs. 12(a) and (b)). At higher speeds, Driver B was applying the brakes between 0.8 and 0.3s before the obstacle (Fig. 12(c)) and removing the foot off the brake pedal while passing over the “anomaly”.

On the other hand, Driver C, at low and medium speeds, was braking 0.6-0.7s before the road “anomaly” (Figs.12 (d) and (e)) and again applying the brakes 0.9 sec after the road “anomaly”. Driver C was re-applying the brakes when the rear wheels of the vehicle hit the “anomaly”. At medium speeds (Fig. 12(e)) braking was occurring just before the road “anomaly”, while at higher speeds (Fig. 12(f)) braking was

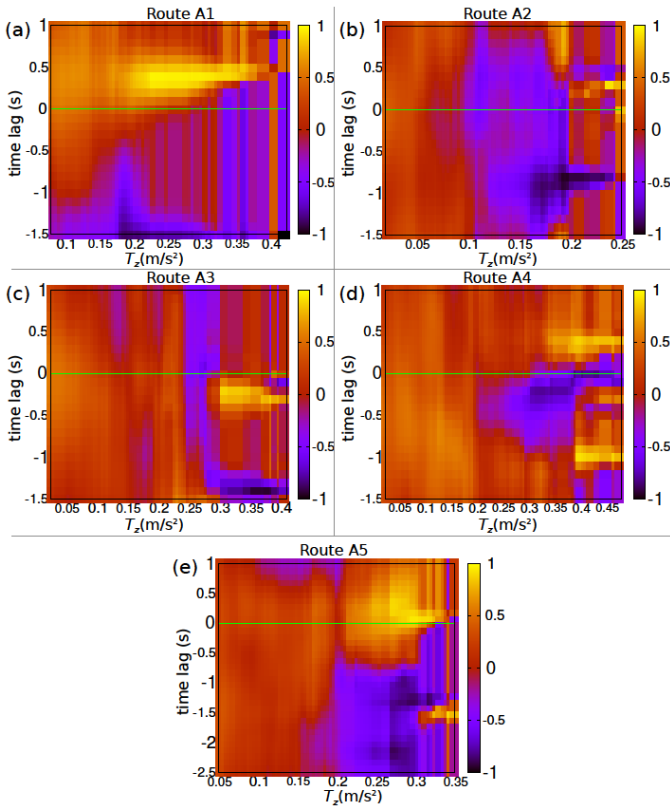


Fig. 11. (color online) Sliding correlation coefficient diagrams (color axis) of the first experiment with respect to different thresholds ( $T_z$ ) of ADF filter of the Z-axis accelerometer data and time lag. The horizontal green line corresponds to zero time lag.

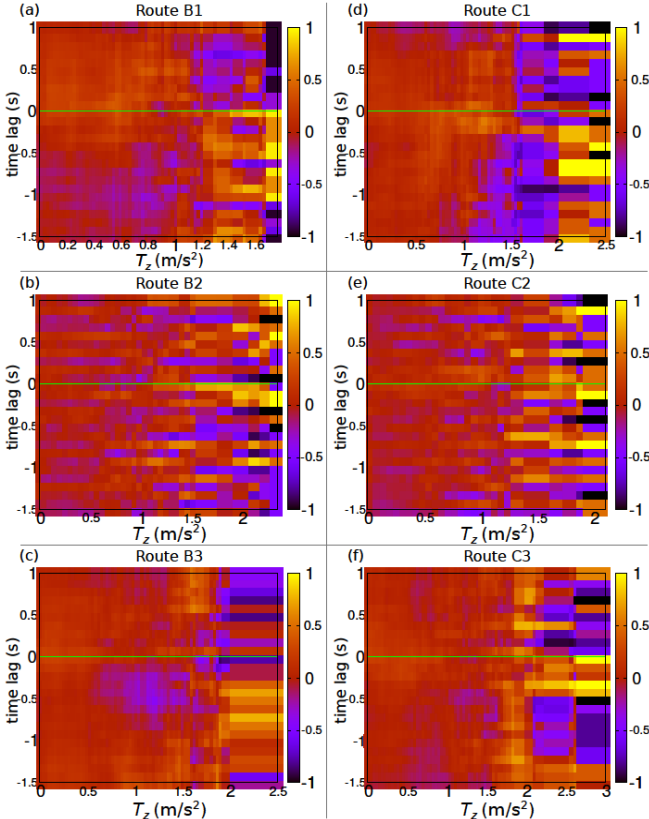


Fig. 12: (color online) Sliding correlation coefficient diagrams (color axis) of the second experiment with respect to different thresholds ( $T_z$ ) of ADF filter of

the Z-axis accelerometer data and time lag. The horizontal green line corresponds to zero time lag.

taking place just before and while passing over the obstacle. At higher speeds, Driver C was not applying the brakes when the rear wheels hit the “anomaly”; a reasonable reaction of a driver that aims to keep the average speed high (Fig. 12(f)).

### Experiment 3:

The purpose of the third experiment was to evaluate the method’s performance using naturalistic driving studies. Two different drivers were asked to track Coventry City’s entry routes (drivers (E1 with Driver E and F2, F3, F4 with Driver F)). The results are presented in Fig. 13. We can see once again, that it was possible to discover the drivers’ braking patterns.

Table I presents the characteristics of each route. The field trials were carried out in a wide range of average speeds and road slope variation. The results indicate that the proposed method is a robust tool for identifying the braking “signature” of drivers and identifying their braking preferences in the occurrence of different road anomalies.

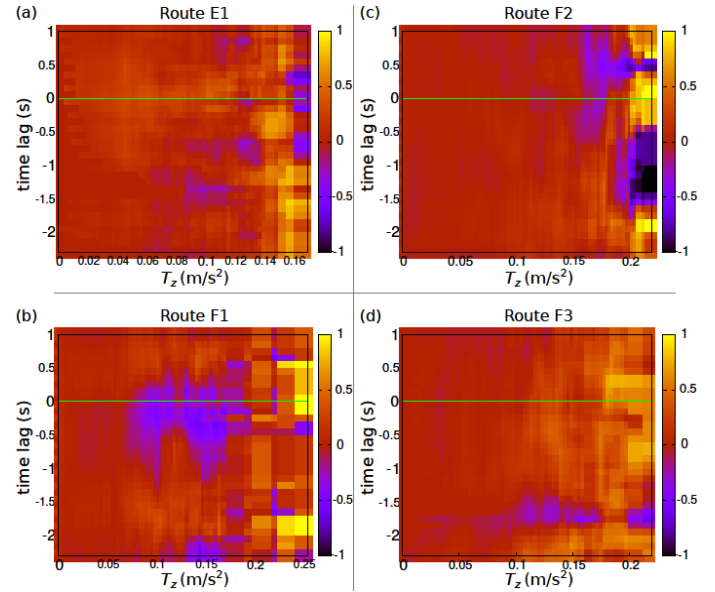


Fig. 13: (color online) Sliding correlation coefficient diagram (color axis) of the entry routes at Coventry City with respect to different thresholds ( $T_z$ ) of ADF filter of the Z-axis accelerometer data and time lag. The horizontal green line corresponds to zero time lag.

TABLE I  
DRIVING ANALYTICS IN EXPERIMENTS 1, 2 AND 3

Experiment 1: Location Coventry, UK							
Route	AvS	StdS	MaxS	AvD	StdD	MaxD	VoA
A1	6.90	2.40	9.36	0.29	0.52	3.62	10
A2	5.84	1.67	8.85	0.33	0.32	1.68	10
A3	5.39	2.29	10.12	0.68	0.71	3.31	10
A4	6.17	2.03	11.19	0.63	0.65	3.31	10
A5	6.50	1.84	10.19	0.66	0.78	3.35	10
Experiment 2: Location Politechniopolis, Zografos, Greece							
Route	AvS	StdS	MaxS	AvD	StdD	MaxD	VoA
B1	5.69	1.24	8.64	0.83	0.64	2.66	57
B2	7.96	1.77	11.93	1.02	0.78	3.04	57
B3	9.52	3.99	15.40	1.34	1.66	7.21	57

C1	5.37	1.64	8.22	0.83	0.72	3.10	57
C2	7.58	2.38	12.89	1.75	1.20	4.89	57
C3	9.86	3.04	19.11	1.22	1.56	8.20	57
<b>Experiment 3:</b>							
<b>Zografos-Iliissia, Greece</b>							
Route	AvS	StdS	MaxS	AvD	StdD	MaxD	VoA
D1	7.21	3.93	16.41	1.07	1.09	6.65	135
<b>Coventry City entry routes</b>							
E1	10.99	6.25	23.44	0.84	0.82	4.15	12
F2	7.02	4.24	16.28	0.38	0.36	1.90	27
F3	6.65	5.16	18.31	0.38	0.38	2.18	37
F4	7.31	5.09	19.70	0.35	0.37	3.38	55
AvS: Average Speed (m/s)							
StdS: Standard deviation of Speed (m/s)							
MaxS: Max Speed (m/s)							
AvD: Average GPS deceleration (m/s <sup>2</sup> )							
StdD: Standard deviation of GPS deceleration (m/s <sup>2</sup> )							
MaxD: Max GPS deceleration (m/s <sup>2</sup> )							
VoA: Variation of Altitude (m)							

## VI. CONCLUSIONS

The widespread use of smartphones can facilitate the large-scale and rapid deployment of Intelligent Transportation Applications. However, the fewer and lower quality signals obtained using a smartphone, compared to the ones available on board, pose a challenge to their exploitation. Furthermore, the uncertainties involved in modeling – due to the variety of vehicles and smartphones – and difficulty in applying rigorous calibration methods, often found in scientific experiments, require the development of agile and adaptive methods. In this paper, a method for automatically learning, using smartphones, driver braking preferences for different types of road anomalies and speeds is presented. The proposed method can be potentially used in a crowd-sensing context for informing and updating navigation maps. The overall aim is to improve driver experience when preview map information is utilized.

The determination of the marked changes of driver's speed and the road anomalies was achieved using a novel Deep Neural Network architecture, suitable for the analysis and correlation of multivariate time series data. Extensive field trials were conducted to validate and test the method. The detection method was evaluated by employing the Receiver Operating Characteristics and the analysis proves its high level of efficiency. The true positive rate was 91.5% and the false positive rate 3%. Furthermore, for the first time, a new technique for discovering driver behavior by applying the sliding correlation coefficient is presented. The proposed visualization scheme reveals the driver's reaction profile when approaching different types of road anomalies. The results using five different driving styles confirm that this new technique is a new formula for the estimation of driver behavior.

The method can be applied in other cases as well, for example in discovering the braking "signature" of drivers when approaching a turn. To further improve the method's performance, we will explore neural network training methods considering also the ROC analysis outcome, not just the mean squared error. In the future, we intend to extend the present study by investigating the driver behavior predictive capability of the proposed Deep Neural Network.

## ACKNOWLEDGMENT

The authors would like to thank Intelligent Variable Message Systems (iVMS), funded by the Government's Local Growth Fund through Coventry and Warwickshire Local Enterprise Partnership. We also would like to thank Georgios Chrysakis and Charis Chaidoutis for helping in the data collection.

## REFERENCES

- [1] A. Klausner, A. Trachtenberg, D. Starobinski, and M. Horenstein, "An Overview of the Capabilities and Limitations of Smartphone Sensors," *Int. J. Handheld Comput. Res.*, vol. 4, no. 2, pp. 69–80, 2013.
- [2] "10 Sensors of Galaxy S5: Heart Rate, Finger Scanner and more."
- [3] R. N. Mitra and D. P. Agrawal, "5G mobile technology: A survey," *Spec. Issue Gener. 5G6G Mob. Commun.*, vol. 1, no. 3, pp. 132–137, Dec. 2015.
- [4] R. Williams, "7 in 10 of world's population using smartphones by 2020," 03-Jun-2015.
- [5] J. Engelbrecht, M. J. Booyen, G. J. van Rooyen, and F. J. Bruwer, "Survey of smartphone-based sensing in vehicles for intelligent transportation system applications," *IET Intell. Transp. Syst.*, vol. 9, no. 10, pp. 924–935, 2015.
- [6] Johnson, D.A. & Trivedi, M.M. 2011, "Driving style recognition using a smartphone as a sensor platform", *IEEE Conference on Intelligent Transportation Systems, Proceedings, ITSC*, pp. 1609, 24
- [7] Singh, G., Bansal, D. & Sofat, S. 2017, "A smartphone based technique to monitor driving behavior using DTW and crowdsensing", *Pervasive and Mobile Computing*, vol. 40, pp. 56-70.
- [8] B. Predic and D. Stojanovic, "Enhancing driver situational awareness through crowd intelligence," *Expert Syst. Appl.*, vol. 42, no. 11, pp. 4892–4909, Jul. 2015.
- [9] G. Castignani, T. Derrmann, R. Frank, and T. Engel, "Driver Behavior Profiling Using Smartphones: A Low-Cost Platform for Driver Monitoring," *IEEE Intell. Transp. Syst. Mag.*, vol. 7, no. 1, pp. 91–102, Spring 2015.
- [10] C. Saiprasert and W. Pattara-Atikom, "Smartphone Enabled Dangerous Driving Report System," in 2013 46th Hawaii International Conference on System Sciences, 2013, pp. 1231–1237.
- [11] Wahlström, J., Skog, I. & Händel, P. 2015, "Driving behavior analysis for smartphone-based insurance telematics", *WPA 2015 - Proceedings of the 2nd Workshop on Physical Analytics*, pp. 19.
- [12] A. Vittorio, V. Rosolino, I. Teresa, C. M. Vittoria, P. G. Vincenzo, and D. M. Francesco, "Automated Sensing System for Monitoring of Road Surface Quality by Mobile Devices," *Transp. Can We More Resour. – 16th Meet. Euro Work. Group Transp. – Porto 2013*, vol. 111, pp. 242–251, Feb. 2014.
- [13] V. Astarita et al., "A Mobile Application for Road Surface Quality Control: UNIQUALROAD," *Proc. EWGT2012 - 15th Meet. EURO Work. Group Transp. Sept. 2012 Paris*, vol. 54, pp. 1135–1144, Oct. 2012.

- [14] V. Gikas and H. Perakis, "Rigorous Performance Evaluation of Smartphone GNSS/IMU Sensors for ITS Applications," *Sensors*, vol. 16, no. 8, 2016.
- [15] Koivisto, M., Costa, M., Hakkarainen, A., Leppänen, K. & Valkama, M. 2016, "Joint 3D positioning and network synchronization in 5G ultra-dense networks using UKF and EKF", 2016 IEEE Globecom Workshops, GC Wkshps 2016 – Proceedings
- [16] E. I. Vlahogianni and E. N. Barmponakis, "Driving analytics using smartphones: Algorithms, comparisons and challenges," *Transp. Res. Part C Emerg. Technol.*, vol. 79, pp. 196–206, Jun. 2017.
- [17] S. Kanarachos and A. Kanarachos, "Intelligent road adaptive suspension system design using an experts' based hybrid genetic algorithm," *Expert Syst. Appl.*, vol. 42, no. 21, pp. 8232–8242, Nov. 2015.
- [18] S. Kanarachos, J. Mathew, A. Chroneos, and M. E. Fitzpatrick, "Anomaly detection in time series data using a combination of wavelets, neural networks and Hilbert transform," presented at the 6th IEEE International Conference on Information, Intelligence, Systems and Applications (IISA2015), Corfu, Greece, 2015.
- [19] S. Kanarachos, S.-R. G. Christopoulos, A. Chroneos, and M. E. Fitzpatrick, "Detecting anomalies in time series data via a deep learning algorithm combining wavelets, neural networks and Hilbert transform," *Expert Syst. Appl.*, vol. 85, pp. 292–304, 2017.
- [20] P. Mohan, V. N. Padmanabhan, and R. Ramjee, "Nericell: Rich Monitoring of Road and Traffic Conditions Using Mobile Smartphones," in *Proceedings of the 6th ACM Conference on Embedded Network Sensor Systems*, New York, NY, USA, 2008, pp. 323–336.
- [21] M. Perttunen et al., "Distributed Road Surface Condition Monitoring Using Mobile Phones," in *Ubiquitous Intelligence and Computing: 8th International Conference, UIC 2011, Banff, Canada, September 2-4, 2011. Proceedings*, C.-H. Hsu, L. T. Yang, J. Ma, and C. Zhu, Eds. Berlin, Heidelberg: Springer Berlin Heidelberg, 2011, pp. 64–78.
- [22] V. Douangphachanh and H. Oneyama, "A study on the use of smartphones under realistic settings to estimate road roughness condition," *EURASIP J Wirel Commun Netw*, vol. 2014, no. 1, p. 114, 2014.
- [23] D. Rajamohan, B. Gannu, and K. Rajan, "MAARGHA: A Prototype System for Road Condition and Surface Type Estimation by Fusing Multi-Sensor Data," *ISPRS Int. J. Geo-Inf.*, vol. 4, no. 3, pp. 1225–1245, Jul. 2015.
- [24] M. Långkvist, L. Karlsson, and A. Loutfi, "A review of unsupervised feature learning and deep learning for time-series modeling," *Pattern Recognit. Lett.*, vol. 42, pp. 11–24, 2014.
- [25] S. Avdaković and N. Čišija, "Wavelets as a tool for power system dynamic events analysis – State-of-the-art and future applications," *J. Electr. Syst. Inf. Technol.*, vol. 2, no. 1, pp. 47–57, May 2015.
- [26] J. C. Goswami and A. E. Hoefel, "Algorithms for estimating instantaneous frequency," *Signal Process.*, vol. 84, no. 8, pp. 1423–1427, Aug. 2004.
- [27] T. Fawcett, "An introduction to ROC analysis," *Pattern Recogn Lett*, vol. 27, pp. 861–874, 2006.
- [28] N. V. Sarlis, S.-R. G. Christopoulos, and M. M. Bemplidaki, "Change  $\Delta S$  of the entropy in natural time under time reversal: Complexity measures upon change of scale," *EPL*, vol. 109, no. 1, p. 18002, 2015.
- [29] N. V. Sarlis and S.-R. G. Christopoulos, "Visualization of the significance of Receiver Operating Characteristics based on confidence ellipses," *Comput Phys Commun*, vol. 185, pp. 1172–1176, 2014.
- [30] C. Spearman, "The Proof and Measurement of Association between Two Things," *Am. J. Psychol.*, vol. 15, no. 1, pp. 72–101, 1904.



#### **Stavros-Richard Christopoulos**

received the BSc in Physics from the National and Kapodistrian University of Athens in 2007 and MSc from the National Technical University of Athens in 2009. He received his PhD degree in the Physics of complex dynamical systems from National and Kapodistrian University of Athens in 2014. He has worked at the National and Kapodistrian University of Athens in Greece and Coventry University in

the UK. His research interests include Deep Neural Networks, Intelligent Transportation Systems, Natural Time Analysis, Statistical Physics and Materials Physics.



#### **Stratis Kanarachos**

received the Diploma in Mechanical Engineering in 2001 and the Ph.D. degree in 2004 from the National Technical University of Athens. He has worked at Frederick University with the Mechanical Engineering Department, Cyprus (2005-2012) and at TNO with the Integrated Vehicle Safety Department, Netherlands (2012-

2014). He is currently a Reader at Coventry University with the School of Engineering, Environment & Computing. His research interests include Deep Temporal Neural Networks, Self-Learning Systems & Training of Neural Networks.



#### **Professor Alexander Chroneos**

is a Professor in Material Physics at Coventry University and an Honorary Reader (2015-today) at Imperial College London. Alex previously worked as a Reader at Coventry university (2014-2015), Lecturer in Energy at The Open University (2012-2014). Alex gained a PhD from Imperial College London (2008), an MSc in Theoretical Chemistry from Oxford

University, BEng in Materials Physics at Imperial College London and BEng in Civil Engineering at Edinburgh University. Alex is the author of more than 200 scientific papers and 3 book chapters.